Arnoldi Algorithm for the Simulation of Multidimensional Infrared Spectroscopy

Tomoyuki Hayashi and Shaul Mukamel*

Department of Chemistry, University of Rochester, Rochester, NY 14627-0216, USA
Received April 14, 2003

The cubic and quartic anharmonic force field of malonaldehyde is calculated using density functional theory at the B3LYP/6-31G(d,p) level, and used to simulate coherent infrared vibrational spectra. 12 normal modes are included in the simulation, and the Arnoldi method is employed for the diagonalization of the Hamiltonian. The calculated three pulse infrared signals in the $\mathbf{k}_1 + \mathbf{k}_2 - \mathbf{k}_3$ direction show signatures of the intramolecular hydrogen bond couplings between the C=O stretch, H-O-C bend and O-H stretch vibrations.

Key Words : Arnoldi algorithm, Infrared spectroscopy, Malonaldehyde, Hydrogen bonding

Introduction

Nonlinear infrared (IR) spectroscopies provide detailed information on molecular structures and their time evolution on the subpicosecond timescale.[1,2] These techniques therefore provide a powerful tool for exploring the structure and proton transfer dynamics in hydrogen bonded systems.

In previous studies, we constructed a vibrational exciton Hamiltonian expanded to quartic order in a subset of internal coordinates of a metal carbonyl complex RDC and obtained a good agreement with experiment.[3] In the present work, the vibrational exciton Hamiltonian is expanded in the normal coordinates and the Implicit Restate Arnoldi Method (IRAM) is used for the diagonalization of the Hamiltonian matrix. This allows us to handle a large Hamiltonian matrix and describe the spectroscopy of large molecules with many vibrational coordinates.

We have calculated three pulse infrared signals of Malonaldehyde (MA). MA is a prototype for intramolecular proton transfer, and its structure and dynamics have been the focus of several experimental and theoretical investigations over the past two decades.[4,12] Infrared experiments show that the structure is planar and asymmetric (Figure 1).[4,5] Microwave spectroscopic studies of Wilsons group[7,8] and others[6,9] suggest that proton transfer occurs *via* tunneling of a hydrogen atom between two oxygens. An *ab Initio* molecular dynamics study at 500 K implied a sub ps proton transfer.[10] The ab Initio potential energy surface (PES) for intramolecular proton transfer has been reported.[11,12]

In the present work we compute the cross peaks in infrared four-wave mixing, induced by anharmonic couplings between the C=O stretch, H-O-C bend and O-H stretch vibrations related to the intramolecular hydrogen bonding.

Vibrational Hamiltonian and the *Ab Initio* Force Field

Geometry optimization and normal mode calculations of MA were executed at the B3LYP/6-31G(d,p) level using Gaussian 98.[13] The potential energy V was expanded around the equilibrium geometry to quartic order in a selected set of normal coordinates Q_k. The Hamiltonian is,
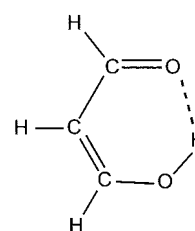

Figure 1. Equilibrium structure of MA. Intramolecular hydrogen bonding is marked by the dotted line.

$$H = \sum_i^{3N-6} \frac{P_i^2}{2m_i} + \frac{1}{2} \sum_i^{3N-6} f_{ii} Q_i^2 + \frac{1}{6} \sum_{i,j,k}^{3N-6} f_{ijk} Q_i Q_j Q_k$$
$$+ \frac{1}{24} \sum_{i,j,k,l}^{3N-6} f_{ijkl} Q_i Q_j Q_k Q_l \tag{1}$$

$$f_{ij} = (\partial^2 V / \partial Q_i Q_j)_{eq} \tag{2}$$

$$f_{ijk} = (\partial^3 V / \partial Q_i Q_j Q_k)_{eq} \tag{3}$$

$$f_{ijkl} = (\partial^4 V / \partial Q_i Q_j Q_k Q_l)_{eq}, \tag{4}$$

where $(\ )_{eq}$ represents the derivatives taken at the equilibrium geometry. The expansion may be carried out using either cartesian, internal, or normal coordinates.[3] Expressing the force field in local coordinates is most suitable for transferring parameters among different systems. However, the kinetic energy in eq. (1) is not then diagonal and is given by the matrix:

$$K = \dot{\mathbf{s}}^T \mathbf{G}^{-1} \dot{\mathbf{s}}, \tag{5}$$

where $\mathbf{s}$ represents the column vector of local coordinates, $\mathbf{s}^T$ is its transpose, and $\mathbf{G}$ is Wilson's $\mathbf{G}$-matrix.[14] The off-diagonal elements of $\mathbf{G}$ were neglected in a previous study.[3] The normal coordinates are most suitable for the simulation of linear and nonlinear vibrational spectroscopy; using these coordinates, both the kinetic energy and the quadratic force fields are diagonal and we can cleanly separate the selected set of coordinates from all others to quadratic order. Moreover, the vibrational exciton Hamiltonian is block diagonal for normal coordinates with different symmetries.

The cubic and quartic anharmonic force constants were determined numerically by computing first and second derivatives of analytical quadratic force constants with 3-point central difference formulas.[15] The quartic expansion coefficients involving 4 different normal coordinates are small compared to the other terms and were neglected. The analytic quadratic force constants in normal coordinates at the distorted geometry along the normal mode Q_k ($\tilde{\mathbf{F}}_{k\pm}$) are obtained by

$$\tilde{\mathbf{F}}_{k\pm} = \mathbf{U}_{eq}^T \mathbf{F}_{k\pm} \mathbf{U}_{eq} \quad (k = 1, ..., 3N-6), \tag{6}$$

where

$$(\tilde{\mathbf{F}}_{k\pm})_{ij} \equiv (\partial^2 V/\partial Q_i Q_j)_{\pm\delta_k} \tag{7}$$

$$(\mathbf{F}_{k\pm})_{ij} \equiv (\partial^2 V/\partial X_i X_j)_{\pm\delta_k} \tag{8}$$

$$(\mathbf{U}_{eq})_{ij} \equiv (\partial X_i/\partial Q_j)_{eq}, \tag{9}$$

and $\mathbf{U}_{eq}^T$ represents the transposed matrix of $\mathbf{U}_{eq}$. X_i is a cartesian coordinate, $(\ )_{\pm\delta_k}$ represents the derivatives taken at the position displaced in $+$ and $-$ directions along the normal coordinate Q_k. The displacement δ was set to 0.02 Bohr (0.0106 Å).

Computing The Vibrational States

The vibrational Hamiltonian was recast using normally ordered Bosonic creation (B_k^+) and annihilation (B_k) operators and expanded in a harmonic basis set of products of local harmonic oscillators ($|m_1 m_2 \ldots m_n\rangle = \Pi_k |m_k\rangle$) following the procedure described earlier.[3] The vibrational eigenstates were obtained by diagonalizing the Hamiltonian matrix with the dimension $(n + m)!/(m!n!)$, where m is the number of modes included and n is the total number of vibrational quanta. This number increases exponentially with n and m, and only a very limited number of normal modes can be handled by standard diagonalization methods. However, we note that the Hamiltonian matrix is very sparse because all the matrix elements between two basis states which differ by more than 4 quanta vanish,

$$H_{ij} = 0 \quad \text{if} \quad \sum_{n=1}^{m} |v_{i,n} - v_{j,n}| > 4, \tag{10}$$

where $v_{i,n}$ represents the number of vibrational quanta on the n'th normal mode in the i'th basis state. To save memory, the coordinate storage format was therefore used for the Hamiltonian matrix.[16] In that format, matrix elements are represented by three 1-dimensional arrays, $val(nnz)$ in which the value of each matrix element is stored, $ind\_x(nnz)$ and $ind\_y(nnz)$ which represent rows and columns of these elements. Each array has the dimension of the number of nonzero elements of the matrix (nnz).

Furthermore, only a small number of the lowest eigenvalues and corresponding eigenvectors are needed because we are interested only in low lying vibrational states which can be excited by infrared light. Therefore the Implicit Restarted ARNOLDI Method (IRAM)[17] was used for diagonalization

Table 1. Vibrational state frequencies (in cm^{-1}) of CO_2 calculated using the normal mode basis including all the internal coordinates are compared with experiment. The numbers in parenthesis represent the number of quanta on the symmetric stretch, bending, and anti-symmetric stretch mode from left to right

Exciton State	Eigenvector	Calc.	Exp.[a]
2	1.0 (010)	651.0	667.4
3	0.5 (100) − 0.8 (020)	1282.0	1285.4
4	0.8 (100) + 0.5 (020)	1367.5	1388.2
5	0.6 (110) − 0.8 (030)	1910.6	1932.5
6	0.8 (110) + 0.6 (030)	2047.5	2076.9
7	1.0 (001)	2361.1	2349.2
15	0.4 (101) − 0.9 (021)	3610.2	3612.8
16	0.8 (101) + 0.4 (021)	3707.0	3714.8

[a]Data from Ref. 22.

of the Hamiltonian. The Arnoldi subroutine was taken from public domain ARPACK package.[17-21] This algorithm is based on the iterated use of the definition of the action of H on a vector v to construct a sequence of vectors from a suitable first guess. The Krylov subspace spanned by these vectors is used to approximate the eigenvectors and eigenvalues. The ARPACK algorithm directly computes a set of eigenvalues and eigenvectors using the implicitly restarted Arnoldi method (IRAM). In our calculation, 25 normal modes and 4 vibrational quanta ($23{,}751 \times 23{,}751$ Hamiltonian matrix) can be included on 256 MB RAM PC.

To test the accuracy of this method, we calculated the vibrational states of CO_2 using the vibrational exciton model in the normal mode basis including all 4 internal coordinates and compared them with experiment.[22] The B3LYP/6-31+ G(d) level was employed for the calculation. The calculated and experimental frequencies of the exciton states are summarized in Table 1. The energy splittings due to the Fermi resonance calculated based on normal mode basis are 85.5 cm^{-1} for {(100),(020)}, 137.9 cm^{-1} for {(110),(030)}, and 96.8 cm^{-1} for {(101),(021)}, and they are in very good agreement with the experimental values of 102.8 cm^{-1}, 144.4 cm^{-1}, and 102.0 cm^{-1}. We found the vibrational exciton states generated from the local mode coordinates to be much less accurate.

Vibrational Spectra of Malonaldehyde

All 12 normal modes with frequency above 1000 cm^{-1} in A' symmetry (in-plane mode) were included in our study. We adopted the following three criteria in constructing the vibrational exciton basis. First, all states with 4 vibrational quanta are included, which is the minimum requirement for quantitative prediction of the eigenvalues and the eigenvectors of the single and double exciton states. Second, all basis states with up to 6 quanta and total energy below 8000 cm^{-1} were included. Third, all states having up to fifth order coupling with the fundamental of v_{17} (C=O stretch) are included in order to reproduce the C=O stretch overtone ($v = 2$) frequency more accurately. These criteria resulted in 7233 exciton states. The 7233×7233 Hamiltonian matrix was
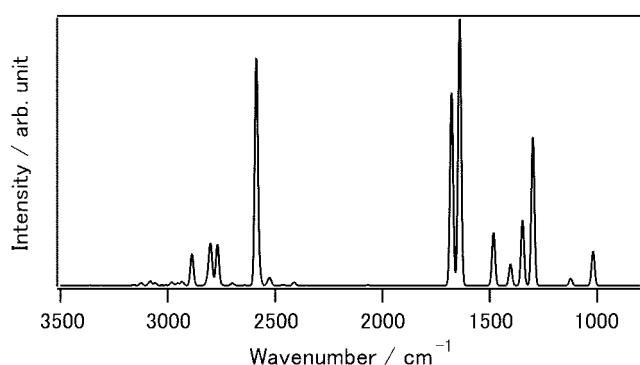
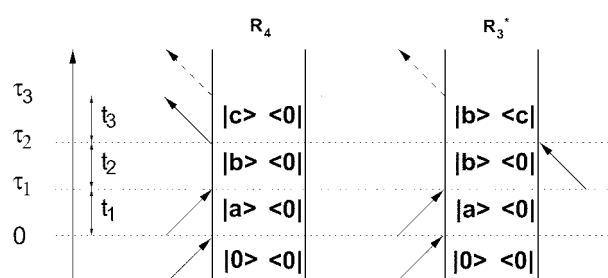**Figure 2**. Simulated linear infrared absorption spectra of MA.

Figure 3. Double-sided Feynman diagrams describing the third-order response in the direction $\mathbf{k}_{III} = \mathbf{k}_1 + \mathbf{k}_2 - \mathbf{k}_3$.

constructed and diagonalized to obtain the 553 eigenvalues below 5900 cm^{-1} and corresponding eigenvectors. The IR intensities were calculated from the dipole moment derivative with respect to the mass-weighted normal coordinates.

The calculated linear infrared absorption spectrum is shown in Figure 2. The peak frequencies are presented in Table 2 and compared with experiment. With few exceptions, the calculated peak positions from the vibrational exciton model are shifted to lower frequency compared to the harmonic ones. v_{12} and v_{13} have a quartic resonance and mixed with each other in the exciton calculation. The calculated H-O-C bend (v_{16}) and C=O stretch (v_{17}) peaks are in good agreement with experiment, but the O-H stretch (v_{19}) frequency is lower than experiment. This is due to overestimating the cubic couplings between v_{19} and the overtone of v_{14}, the combination band of v_8 and v_{15}, v_{11} and v_{14}, and v_{13} and v_{14}. This can be attributed to the lack of convergence of the Taylor expansion of the PES around the equilibrium geometry. The tunneling barrier height of proton transfer is estimated to be very low (42 kJmol^{-1} [23]) and quartic force field could not model this PES with a sufficient accuracy. Including a quintic (f_{ijklm}) and sextic (f_{ijklmn}) force field should improve the accuracy of the peak position. However, in order to reproduce the experimental tunneling vibrational splitting

(21.8 cm^{-1}), the double-well potential along the proton transfer coordinate should be modelled explicitly.[11] This goes beyond the scope of this work.

We have calculated the three pulse infrared signal of MA generated in the direction $\mathbf{k}_{III} = \mathbf{k}_1 + \mathbf{k}_2 - \mathbf{k}_3$ with ZZZZ polarization configuration using the sum over states expression[24] and orientational factors in Eq. 13 of Reference.[25] The response function is given by the sum of two types of Liouville space pathways,

$$R(t_3, t_2, t_1) = R_4(t_3, t_2, t_1) - R_3^*(t_3, t_2, t_1). \quad (11)$$

The Liouville space paths are represented by the double-sided Feynman diagrams shown in Figure 3 where state *a*, *b* and *c* correspond to one of the vibrational exciton states. The signal in the frequency domain is obtained by,

$$S(t_1, \omega_2, \omega_3) = \int_{-\infty}^{\infty} dt_3 \int_{-\infty}^{\infty} dt_2 R(t_3, t_2, t_1)$$
$$\times \exp(-i(\omega_3 t_3 + \omega_2 t_3)). \quad (12)$$

The incident pulses were assumed to have a broad bandwidth of ~400 cm^{-1}. A homogeneous linewidth of 3 cm^{-1} was taken for all transitions.

The signal for the three incident pulses tuned to 1678, 1480 and 1480 cm^{-1} is displayed in Figure 4. We found 339
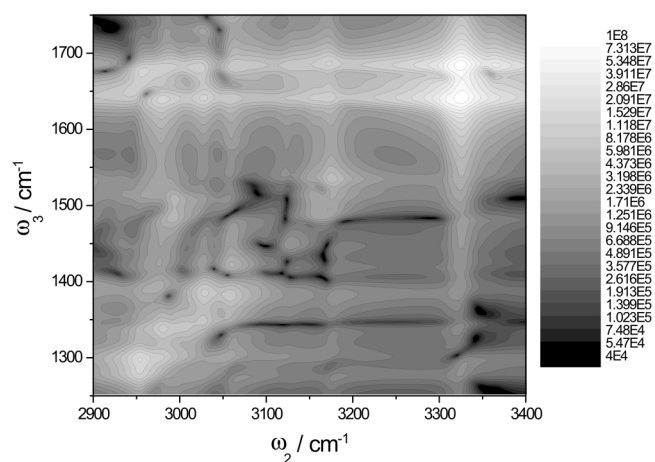
Table 2. Frequencies (in cm^{-1}) obtained from the vibrational exciton model are compared with harmonic normal mode calculations and with experiment

Exciton State		Normal Mode			Exp.[a]
Level	Frequency	Mode	Description	Frequency	
2	1019.0	v_8		1018.8	
3	1123.6	v_{11}		1122.3	1092
4	1299.3	v_{12}		1302.3	1260
5	1347.6	v_{13}		1405.6	
6	1403.6	v_{14}		1419.2	1358
7	1482.6	v_{15}		1490.7	1452
8	1640.3	v_{16}	H-O-C bend	1654.8	1593
9	1678.0	v_{17}	C=O stretch	1718.1	1655
20	2587.3	v_{18}	O-H stretch	3042.8	2960
29	2801.1	v_{19}	C-H stretch	2991.2	
41	3058.2	v_{20}	C-H stretch	3181.8	3100
45	3124.0	v_{21}	C-H stretch	3237.6	

[a]Data from Ref. 4.

Figure 4. Three pulse infrared signal (absolute value of $S(t_1 = \omega_2, \omega_3)$ (Eq. 12)) of MA in the $\mathbf{k}_{III}$ direction. The three 24 fsec incident pulses are tuned at 1678, 1480 and 1480 cm^{-1} and have a bandwidth of 420 cm^{-1}.

Table 3. Frequencies and corresponding Liouville space pathways (in cm^{-1}) of the peaks in Figure 4 and 5. The Liouville space pathway is specified by the diagram, R_4 or R_3^* and the states a, b and c in Figure 3. a, b and c correspond to one of the vibrational exciton states in Table 4

Peak (ω_2, ω_3)	Liouville Space Pathway			
	Diagram	a	b	c
(3326,1640)	R_4	8	51	8
(3326,1686)	R_3^*	8	51	8
(3361,1678)	R_4	9	52	9
(3361,1683)	R_3^*	9	52	9
(2953,1678)	R_4	8	36	9
(2953,1275)	R_3^*	8	36	9
(3326,2587)	R_4	8	51	20
(3361,2587)	R_4	9	52	20

Table 4. Frequencies (in cm^{-1}) and eigenvectors of the exciton states in Table 3. υ_{v_n} represents υ vibrational quanta on the v_n normal mode

Exciton State	Frequency	Eigenvector
8	1640.3	$-0.94\,(1v_{16}) + 0.16\,(1v_{16}1v_{19}) +$
9	1678.0	$+0.93\,(1v_{17}) + 0.18\,(1v_{17}1v_{19}) +$
20	2587.3	$+0.66\,(1v_{19}) + 0.30\,(2v_{19}) +$
36	2953.5	$-0.71\,(1v_{12}1v_{17}) - 0.39\,(1v_{20}) - 0.34\,(1v_{12}1v_{16}) +$
51	3326.4	$-0.93\,(2v_{16}) - 0.14\,(2v_{16}1v_{19}) +$
52	3361.5	$+0.91\,(2v_{17}) + 0.16\,(2v_{17}1v_{19}) +$

peaks generated by different Liouville space pathways. The frequencies of peaks and corresponding Liouville space pathways are summarized in Table 3. The frequencies and the eigenvectors of the related vibrational exciton states are given in Table 4 The strongest peaks at $(\omega_2, \omega_3) = (3326$ cm^{-1}, 1640 cm^{-1}) and (3326,1686) come mainly from R_4 and R_3^* diagrams including the exciton states 8 and 51. The 8 and 51 exciton states are primarily $v = 1$ and $v = 2$ of v_{16} (H-O-C bending mode) (Table 4), and these peaks are
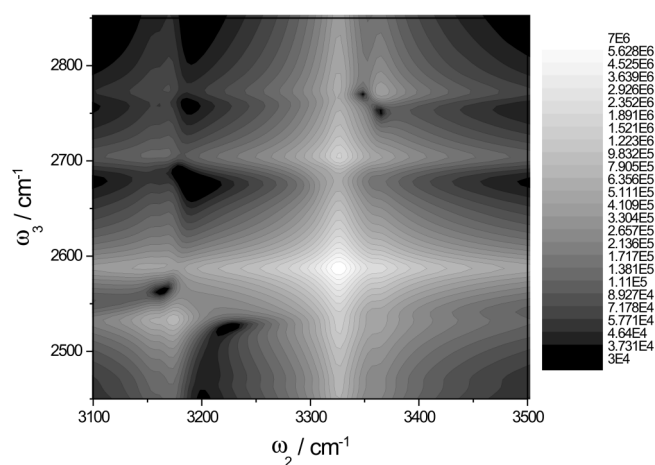

Figure 5. Three pulse infrared signal (absolute value of $S(t_1 = 0, \omega_2, \omega_3)$ (Eq. 12)) of MA in the $\mathbf{k}_{III}$ direction. The three 25 fsec incident pulses are tuned to 1692, 1669 and 774 cm^{-1} and have a bandwidth of 400 cm^{-1}.

generated by transitions between the fundamental and overtone of v_{16}. The next most intense peaks at (3361,1678) and (3361,1683) come from R_4 and R_3^* diagrams involving the transitions between $v = 1$ and $v = 2$ of v_{17} (C=O stretch). The weaker peaks at (2953,1678) and (2953,1275) correspond to R_4 and R_3^* diagrams involving the transitions between v_{17} (C=O stretch) fundamental, v_{19} (O-H stretch) fundamental, and v_{16} (H-O-C bend) fundamental. The intensities of these 2 peaks come from anharmonic (mainly cubic) couplings between v_{17} (C=O stretch), v_{16} (H-O-C bend), and v_{19} (O-H stretch). There are many other peaks resulting from anharmonic couplings between different normal modes.

The $\mathbf{k}_{III}$ signal where the incident pulses are tuned at 1692, 1669 and 774 cm^{-1} is displayed in Figure 5. We found 57 peaks generated by different Liouville space pathways. The strongest peak at (3326,2587) corresponds to the R_4 diagram involving transitions between the v_{16} (H-O-C bend) fundamental, overtone of v_{15} (H-C-C bend), and v_{19} (O-H stretch) fundamental. The Intensity of this peak is related to anharmonic couplings between v_{16} (H-O-C bend), v_{15} (H-C-C bend) and v_{19} (O-H stretch). This peak has a side band at (3361,2587) coming from the R_4 diagram involving the transitions between fundamental v_{17} (C=O stretch), overtone of v_{16} (H-O-C bend), and v_{19} (O-H stretch) fundamental. The intensities of these peaks reflect anharmonic (mainly cubic) couplings between v_{17} (C=O stretch), v_{16} (H-O-C bend), and v_{19} (O-H stretch).

Discussion

We have identified signatures of the intramolecular hydrogen bonding couplings between the C=O stretch, H-O-C bend and O-H stretch vibration in the $\mathbf{k}_{III}$ signal. The short pulses used here generate many peaks corresponding to different Liouville pathways. Assuming a constant density of exciton states, the number of terms should be cubic in the pulse bandwidth. A 300 cm^{-1} bandwidth was reported in mid-infrared region by difference-frequency mixing of two visible phase-locked linearly chirped pulses in GaAs,[26] and broader pulses are expected to be available in the near future.

In order to reproduce the vibrational splitting, the double-well potential along the proton transfer coordinate and its coupling to other intramolecular coordinates should be modelled explicitly. Symmetric mode coupling (SMC) and squeezed double well potential (SQZ) which are two-dimensional model potentials for proton-transfer system proposed by Takada et. al. could be used to that end.[27] It is also important, especially for larger molecules, to describe highly excited low frequency modes correctly. This may be accomplished using curvilinear normal modes and local modes (CNLM) that use the Morse potential as a reference for local stretches and harmonic oscillator for the normal modes.[28]

References

1. Mukamel, S.; Hochstrasser, R. M. *Supecial issure in Chem. Phys.* **2001**, 135.
2. Mukamel, S. *Ann. Rev. Phys.* **2000**, *51*, 691.
3. Moran, A. M.; Dreyer, J.; Mukamel, S. *J. Chem. Phys.* (in press).
4. Seliskar, C. J.; Hoffmann, R. E. *J. Mol. Spectr.* **1982**, *96*, 146.
5. Schiering, D. W.; Katon, J. E. *Appl. Spectr.* **1986**, *40*, 1049.
6. Baba, T.; Tanaka, T.; Morino, I.; Yamada, M. T.; Tanaka, K. *J. Chem. Phys.* **1999**, *10*, 4131.
7. Rowe, W. F.; Duerst, R. W.; Wilson, E. B. *J. Am. Chem. Soc.* **1977**, *99*, 7072.
8. Baughcum, S. L.; Duerst, R. W.; Rowe, W. F.; Smith, Z.; Wilson, E. B. *J. Am. Chem. Soc*. **1981**, *103*, 6296.
9. Firth, D. W.; Beyer, K.; Dvorak, M. A.; Reeve, S. W.; Grushow, A.; Loepold, K. R. *J. Chem. Phys.* **1991**, *94*, 1812.
10. Wolf, K.; Mikenda, W.; Nusterer, E.; Schwarz, K.; Ulbricht, C. *Chem. Eur. J.* **1998**, *4*, 1418.
11. Yagi, K.; Taketsugu, T.; Hirao, K. *J. Chem. Phys.* **2001**, *115*, 10647.
12. Makri, N.; Miller, W. H. *J. Chem. Phys.* **1989**, *91*, 4026.
13. Frisch, M. J.; Trucks, G. W.; Schlegel, H. B.; Scuseria, G. E.; Robb, M. A.; Cheeseman, J. R.; Zakrzewski, V. G.; Montgomery, Jr., J. A.; Stratmann, R. E.; Burant, J. C.; Dapprich, S.; Millam, J. M.; Daniels, A. D.; Kudin, K. N.; Strain, M. C.; Farkas, O.; Tomasi, J.; Barone, V.; Cossi, M.; Cammi, R.; Mennucci, B.; Pomelli, C.; Adamo, C.; Clifford, S.; Ochterski, J.; Petersson, G. A.; Ayala, P. Y.; Cui, Q.; Morokuma, K.; Malick, D. K.; Rabuck, A. D.; Raghavachari, K.; Foresman, J. B.; Cioslowski, J.; Ortiz, J. V.; Baboul, A. G.; Stefanov, B. B.; Liu, G.; Liashenko, A.; Piskorz, P.; Komaromi, I.; Gomperts, R.; Martin, R. L.; Fox, D. J.; Keith, T.; Al-Laham, M. A.; Peng, C. Y.; Nanayakkara, A.; Gonzalez, C.; Challacombe, M.; Gill, P. M.; Johnson, W. B.; Chen, W.; Wong, M. W.; Andres, J. L.; Gonzalez, C.; Head-Gordon, M.; Replogle, E. S.; Pople, J. A. *Gaussian 98 rev. A. 7*; Gaussian, Inc.: Pittsburgh, PA, 1998.
14. Califano, S. *Vibrational States*; John Wiley and Sons: London, 1976.
15. *Encyclopedia of Computational Chemistry*; Schleyer, P.; Allinger, N.; Clark, T.; Gasteiger, J.; Kollman, P. A.; Schaefer III, H. A.; Schreiner, P. R., Eds.; John Wiley and Sons: Chichester, 1998.
16. Remington, K. A.; Pozo, R. *NIST Sparse BLAS Users Guide*; 1996.
17. Lehoucq, R. B., *Ph.D. Thesis*, Rice University: Houston, Texas, 1995.
18. Sorensen, D. C. Technical Report No. TR-96-40.
19. Lehoucq, D. Y. C.; Sorensen, R. B. ARPACK Users Guide: *Solution of Large Scale Eigenvalue Problems by Implicitly Restarted Arnoldi Methods*; 1996.
20. Maschho, K. J.; Sorensen, D. C. P. ARPACK: An Efficient Portable Large Scale Eigenvalue Package for Distributed Memory Parallel Architectures. In Applied Parallel Computing in Industrial Problems and Optimization.
21. *Lecture Notes in Computer Science*; Wasniewski, J.; Dongarra, J.; Madsen, K.; Olesen, D., Eds.; Springer-Verlag: Berlin, 1996; Vol. 1184.
22. Nakagawa, I, *Vibrational Spectroscopy* (in Japanese); Gakkai Shuppan Center, Tokyo, 1987.
23. Sewell, T. D.; Guo, Y.; Thompson, D. L. *J. Chem. Phys.* **1995**, *103*, 8557.
24. Mukamel, S. *Nonlinear Optical Spectroscopy*; Oxford University Press: New York, 1995.
25. Hochstrasser, R. M. *Chem. Phys.* **2001**, *266*, 273.
26. Belabas, N.; Likforman, J.-P. *Optics Letters* **2001**, *26*, 743.
27. Takada, S.; Nakamura, H. *J. Chem. Phys.* **1995**, *102*, 3977.
28. Zhang, Y.; Klippenstein, S. J.; Marcus, R. A. *J. Chem. Phys.* **1991**, *94*, 7319.